PHYSICAL REVIEW E **89**, 061001(R) (2014)

Consecutive turbulence transition delay with reinforced passive control

Sohrab S. Sattarzadeh,[1] Jens H. M. Fransson,[1,*] Alessandro Talamelli,[1,2] and Bengt E. G. Fallenius[1]
[1]*Linné Flow Centre, KTH Royal Institue of Technology, SE-10044 Stockholm, Sweden*
[2]*Dipartimento Ingegneria delle Construzioni Meccaniche, Alma Mater Studiorum, Università di Bologna, I-47100 Forlì, Italy*
(Received 11 April 2014; published 17 June 2014)

Miniature vortex generators (MVGs) are able to delay the transition to turbulence in a flat plate boundary layer if properly designed. Unfortunately, the natural recovery of the modulated laminar base flow in the streamwise direction is of exponential space scale and hence the passive laminar control fades away fairly rapidly. Here we show that by placing a second array of MVGs downstream of the first one it is possible to nourish the counter-rotating streamwise vortices responsible for the modulation, which results in a prolonged streamwise extent of the control. With this control strategy it is possible to delay the transition to turbulence, consecutively, by reinforcing the control effect and with the ultimate implication of obtaining a net skin-friction drag reduction of at least 65%.

DOI: 10.1103/PhysRevE.89.061001 PACS number(s): 47.27.Cn, 47.85.ld, 47.20.Pc, 47.85.lb

Despite the substantial amount of research in the area of fluid mechanics during the past century, the common belief concerning surface roughness was that it inevitably promotes a boundary layer transition to turbulence. Halfway through the past decade a ground breaking result was published proving that organized circular roughness elements can act stabilizing on the flow and hence delay the transition to turbulence with the implication of reducing skin-friction drag [1]. The physical control mechanism rests on the idea of setting up a mean velocity gradient orthogonal to the base flow and parallel to the surface. This leads to an additional term in the perturbation energy equation, which together with the viscous dissipation counteracts the wall-normal production term and hence is able to damp or even nullify the growth of Tollmien-Schlichting (TS) waves [2] otherwise responsible for the transition onset in low-background-disturbance environments [3–5]. A number of both experimental [1,6–9] and numerical [2,10,11] studies have reported on the attenuation of TS waves, using the above control mechanism, but only two of them had hitherto been successful in terms of delaying the transition (see [1,11]).

The circular roughness elements mounted equidistantly in an array on a flat plate and reported in Ref. [1] modulated the two-dimensional boundary layer into regions of alternating high and low speed in the spanwise direction, often denoted streamwise streaks. Such streaks provide the boundary layer with additional, but negative, turbulence production via the mean velocity gradients in the spanwise direction. The generation of steady and stable streamwise streaks, which by themselves do not transition to turbulence, has turned out to be a challenging task from an experimental point of view. While previous studies [2,9,10] suggested that the higher the streak amplitude, the stronger the stabilizing effect is, the streaks themselves became more unstable. The drawback of blocking the flow by means of a solid circular roughness element is that a wake, which is even more unstable than the streaks, will be formed. At a threshold streak amplitude of about 12% of the free stream velocity U_∞ [9], a shedding instability of the wake will set in and cause a rapid breakdown to turbulence of the streaky base flow, which naturally would not be susceptible to secondary instabilities until above 26% [12]. In striving toward generating a high-amplitude streaky boundary layer without forming unstable wakes behind the devices, classical vortex generators traditionally used for separation control became an attractive candidate. Similar to the circular roughness elements, this type of device is passive in the sense that they do not require any energy input to the system to operate; instead they use the existing energy in the flow in order to obtain the control. Furthermore, simple and robust actuators are coveted for real flow applications since they do not need to rely on sensitive electronics as in sensor-actuator control systems. Experimental works by Fransson and Talamelli showed that miniature vortex generators (MVGs) can generate a laminar and stable streaky boundary layer with amplitudes up to 32% [13,14]. Subsequent works [15,16] have shown that MVGs, if properly designed, are coveted devices for transition delay and may accomplish a reduction of the local skin-friction drag coefficient c_f with up to an order of magnitude in the range of high Reynolds numbers.

An important aspect when talking about drag reduction is the energy balance. The skin friction induced by the generated streaks increases with the streak amplitude. A local increase of c_f of about 10% is typical for a streaky boundary layer with high enough amplitude (about 25%) to accomplish a significant transition delay [16]. The local increase in c_f is followed by a decay in the streamwise direction and for the exemplified streaky boundary layer it has fully recovered at around 300 MVG heights downstream of the MVG array [14]. A direct numerical simulation of the flow around a pair of MVGs giving a streak amplitude of about 25% has been performed in order to access the total drag [17]. In the simulation a length of a flat plate of $\mathrm{Re}_x = xU_\infty/\nu = 4.5 \times 10^5$, expressed in terms of Reynolds number, was considered, with x and ν denoting the distance from the leading edge and the kinematic viscosity, respectively. Downstream of this position the modulated boundary layer has recovered and the c_f curve falls on top of the originally-two-dimensional curve. The total drag increase due to the presence of the MVGs amounts to 2.5%, which becomes negligible if the transition would occur without the MVGs, and hence makes the passive control method outlined above remarkably cheap.

*Corresponding author: jensf@kth.se

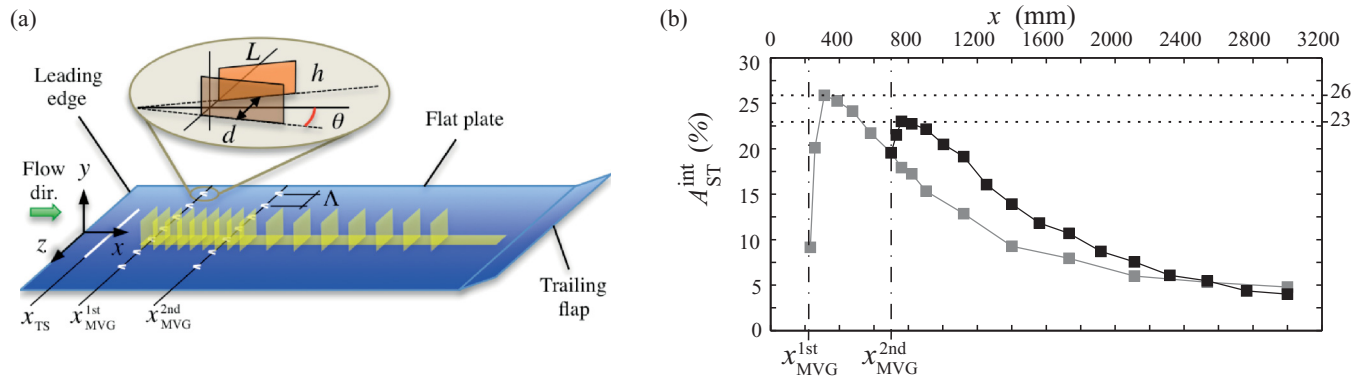

FIG. 1. (Color online) (a) Schematic of the flat plate inside the wind tunnel with the flow from left to right. The TS wave disturbance slot is located at $x_{TS} = 190$ mm, the first array of MVGs at $x^{1st}_{MVG} = 222$ mm, and the second array of MVGs at $x^{2nd}_{MVG} = 700$ mm from the leading edge. The lighter gray (yellow) rectangles depict measurement planes. Both cross-sectional and streamwise planes were taken. The inset is a blowup of a pair of MVGs. Here $h = 1.3$ mm, $L = 3.25$ mm, $d = 3.25$ mm, $\theta = 9°$, and $\Lambda = 14.6$ mm. (b) Streak amplitude A^{int}_{ST} in the presence of the first array of MVGs (gray squares) and both MVG arrays (black squares).

A shortcoming in applying devices localized in the streamwise direction is that the originally-two-dimensional boundary layer will be recovered and the control effect will fade away. The answer to this problem cannot be higher-amplitude streaks, which persist further downstream *per se*, since one may exceed the threshold streak amplitude in the generation process. Beyond this threshold value the streaky base flow transitions to turbulence via a bypass scenario [18] and the control fails. A nontrivial but appealing solution would be to reinforce the stabilizing effect by regenerating the streaky boundary layer after some downstream distance. If this strategy is proven to be effective, the results will be of interest both for technological applications and for offering possibilities for theories on how organisms reduce their drag in an aqueous environment [19,20]. An additional complexity, putting a higher demand on the regeneration process, is the possible presence of nonlinear disturbance waves. This makes it an even more challenging task, which is the subject of the present investigation.

The present measurements were performed in a flat plate boundary layer mounted in the minimum-turbulence-level (MTL) closed-circuit wind tunnel at KTH Mechanics. The dimensions of the test section were $7.0 \times 0.8 \times 1.2$ m^3, corresponding to (length)×(height)×(width). An adjustable ceiling allows setting the external pressure gradient along the plate. Single-point hot-wire anemometry measurements were carried out with a temporal resolution of 5 kHz and a spatial resolution of 0.6 mm, corresponding to the length of the hot-wire probe.

Figure 1 shows a schematic of the flat plate mounted horizontally inside the test section. The coordinate system (x,y,z) is shown on the leading edge and the streamwise velocity component is denoted by U, with a small letter corresponding to the streamwise velocity fluctuation. Unsteady periodic disturbance forcing is introduced into the boundary layer as two-dimensional sinusoidal TS waves at x_{TS}, which amplify as they propagate downstream. The TS waves are excited by means of uniform spanwise blowing and suction through a set of phase-locked computer-driven loudspeakers. The same signal driving the loudspeakers is used to phase trigger the hot-wire measurements and hence the disturbance field can accurately be reconstructed in the linear regime from single-point measurements as performed here. The nondimensional TS frequency F $(= 2\pi f \nu / U_\infty^2 \times 10^6)$ was set to 100 in all experiments to give a large exponentially unstable region (about 840 mm for $U_\infty = 6$ m s^{-1}) between neutral points on the stability curve and to favor the transition to turbulence. Here f is the forcing frequency in hertz.

In the present investigation, three cases, denoted C0, C1, and C2, were analyzed and are shown in Table I: C0 corresponds to the reference two-dimensional base flow, while C1 and C2 correspond to measurements with a single and a double MVG array configuration, respectively, mounted downstream of the disturbance slot as shown in Fig. 1(a). Rectangular bladed MVGs were employed in this study. This type of MVG induces streamwise vortices in the boundary layer similar to the triangular ones [14–16], but with a higher streak amplitude for a fixed MVG array configuration and

TABLE I. Summary of the three experimental cases or configurations with C0 being the reference case without control and C1 and C2 with one and two MVG arrays, respectively. The first and second vector elements appearing in the table correspond to the values resulting from the first and second MVG arrays, respectively.

Case	No. of MVG arrays	U_∞ (m s^{-1})	x_{MVG} (mm)	β^0	Re_h	h/δ_1^0	$A^{int,p}_{ST}$ (%)	F	x_{tr} (mm)
C0	0	6	(,)	(,)	(,)	(,)	(0, 0)	100	1344
C1	1	6	(222,)	(0.32,)	(292,)	(1.03,)	(26, 0)	100	2882
C2	2	6	(222, 700)	(0.32, 0.57)	(292, 181)	(1.03, 0.53)	(26, 23)	100	>4000

U_∞. The characteristics of the MVG arrays are shown in the caption of Fig. 1 and Table I, with β the spanwise wave number scaled by the boundary layer scale $\delta = \sqrt{x\nu/U_\infty}$ and $\mathrm{Re}_h = hU(y=h)/\nu$ the MVG height Reynolds number. Superscript 0 indicates evaluation at the actual $x = x_{\mathrm{MVG}}$ location and δ_1 denotes the displacement thickness.

Cross-sectional yz measurement planes, depicted as yellow rectangles in Fig. 1(a), were captured behind one MVG pair in order to follow the downstream evolution of the modulated streaky boundary layer for both the C1 and C2 cases. Each plane consisted of 20×15 measurement points. An integral streak amplitude measure, taking the full modulation in the cross-sectional plane into account, has been shown to be an appropriate measure in the search for a proper streamwise scaling relating both geometrical parameters of the MVGs and boundary layer parameters to the downstream evolution [16]. This measure is used here to characterize the streamwise evolution and is defined as

$$A_{\mathrm{ST}}^{\mathrm{int}}(x) = \int_{-1/2}^{+1/2} \int_0^{\eta^*} \frac{|U(x,y,z) - U^z(x,y)|}{U_\infty} d\eta\, d\zeta, \quad (1)$$

where $\eta = y/\delta$ and $\zeta = z/\Lambda$. For the integration in the wall-normal direction, the truncation value is set to $\eta^* = 9$ and the superscript z denotes the average in the spanwise direction. Figures displaying the measured cross-sectional planes have been published previously and hence are not shown here with the motivation that the yz planes behind the second MVG array look very similar to the planes behind the first array; interested readers are instead referred to [14–16]. The streamwise streak amplitude initially grows and reaches a peak, where after it appears to decay exponentially [16] [see Fig. 1(b)]. The peak value is often used to characterize the strength of the streaks, here defined as $A_{\mathrm{ST}}^{\mathrm{int,p}}$, and are 26% and 23% behind the first and second MVG array, respectively. Note that this amplitude measure differs from the conventional measure based on the maximum velocity difference in the wall-normal direction as used in the introduction. The integral to the maximum measure is typically related to a factor of about 1.4. Figure 1(b) shows that the regeneration process is successful in terms of being able to reinforce a stable and steady streaky base flow. A failed regeneration would be manifested in a drastic drop of $A_{\mathrm{ST}}^{\mathrm{int}}$ since a turbulent boundary layer would mix the flow and hence break up the streaks, rendering a zero streak amplitude.

Here no attempt has been made to optimize the second MVG array. Hence, for simplicity, the geometry of the second MVG array was kept constant with the same Λ and spanwise phase as the first array, i.e., aligned in the streamwise direction with the first array. With the MVGs aligned in the streamwise direction, the remodulation of the base flow is higher and more robust compared to a staggered configuration [14]. Given these constraints, the downstream location of the second array becomes the only parameter. An important parameter for a successful regeneration of the streaky base flow is Re_h. The higher the Re_h, the stronger the generated vortices are and the higher the obtained streak amplitude becomes. Therefore, the location of the second array plays a fundamental role in the success of the base flow remodulation since a too close placement to the first array may cause unstable streaks and the bypass transition can occur. Conversely, if the distance is too large from the first array, the streak amplitude may not be high enough to attenuate disturbance growth and the onset of the transition may occur.

The base flow modulation and the reconstructed instantaneous disturbance fields (see the caption of Fig. 2) in the xz plane are shown in Figs. 2(a) and 2(b), respectively, for all three cases C0–C2. In Fig. 2(b) the disturbance fields are accurately reconstructed until the transition starts; after that the motion becomes random, which manifests itself as scattered data. This way of plotting the data gives a clear visual inspection of where the transition starts. For the present U_∞ and F, branches I and II of the neutral stability curve are located around $x = 448$ and 1285 mm, respectively, calculated from linear stability

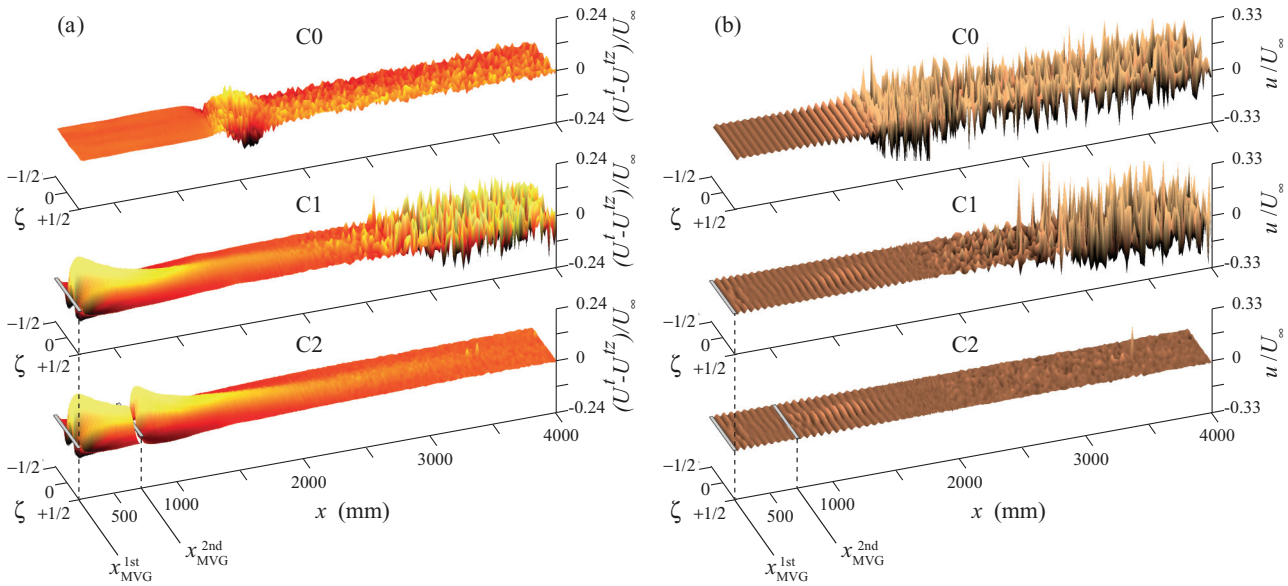

FIG. 2. (Color online) (a) Modulated base flow as $U^t(x,z) - U(x)^{tz}$ and (b) reconstructed instantaneous disturbance field $u = U(x,z,t^*) - U^t(x,z)$ for all three cases C0–C2. Superscripts t and/or z denote averaged dimensions and t^* represents a particular time. The wall-normal distance of the horizontal planes from the flat plate is $y/\delta_1 = 0.5$.

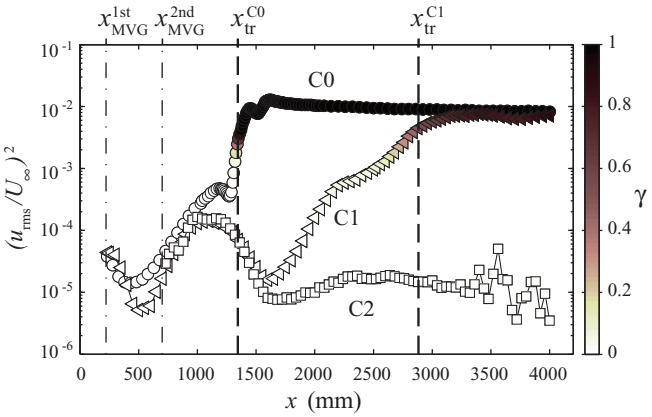

FIG. 3. (Color online) Disturbance energy evolution in the streamwise direction at $y/\delta_1 = 0.5$ and $\zeta = 0$ for the cases C0–C2. The color bar applied to the symbols corresponds to the intermittency γ of the velocity signal.

theory. The initial forcing amplitude of the generated TS waves was kept constant and fairly high, causing the transition to turbulence right after branch II of the neutral stability curve for the C0 case. Figure 2 shows that in the C0 case, i.e., without control, the transition onset is around $x = 1300$ mm from the leading edge. When a first array of MVGs is mounted the distance until transition onset is more than doubled, i.e., around $x = 2900$ mm. With a second array of MVGs the transition onset is not initiated throughout the downstream measured region, i.e., $x > 4000$ mm. An interesting observation, which has been reported previously [9,16], is that the largest TS wave amplification appears on the center line of the downstream measurement, i.e., in a high-speed streak. The growth is observed for both the C1 and C2 cases, but in the C2 case it is not enough to trigger the transition further downstream. The careful reader will note that the base flow modulations Fig. 2(a), in particular for C0 and C1, also show some scatter of data in the downstream direction without justification, since the base flow modulations are based on time-averaged data. The explanation lies in the short sampling time (only 0.5 s at each point) in order to afford the large number of data points ($x \times z = 501 \times 15$ for the C1 case as an example) to resolve the disturbance wavelength in Fig. 2(b). The data shown in Fig. 3, on the other hand, are calculated based on long-time samples, 60, 45, and 15 s for the C0, C1, and C2 cases, respectively, ensuring reliable and statistically converged quantities.

In Fig. 3 the disturbance energy $(u_{rms}/U_\infty)^2$, where rms is the root-mean-square value of the velocity signal, is shown for the three different measurement cases taken along $\zeta = 0$, i.e., in the high-speed streaks. Note that similar results were obtained for other measured spanwise positions. The color bar of the symbols indicates the intermittency of the velocity signal, with values of zero and unity corresponding to a laminar and a turbulent flow, respectively. It is customary to define the transition location x_{tr} where the intermittency value γ is equal to 0.5 [21], which has been done here to obtain $x_{tr}^{C0} = 1344$ mm, $x_{tr}^{C1} = 2882$ mm, and $x_{tr}^{C2} > 4000$ mm. Based on these transition locations, one may estimate the overall drag for all three cases using the Blasius skin-friction relation for the laminar part of the boundary layer and one among the many empirical relations for the turbulent part. For the C0 case the overall drag coefficient amounts to 3.08×10^{-3} down to the reference length $x = 4000$ mm. The C1 case has an overall drag coefficient, including the induced drag by the MVGs themselves, of 1.89×10^{-3}, which amounts to a net drag reduction of 39%. When considering the C2 case down to the same reference length, including the drag induced by two arrays of MVGs, the overall drag coefficient becomes 1.08×10^{-3}, corresponding to a net reduction of 65% compared to the uncontrolled C0 case. One should keep in mind that this figure is a minimum net drag reduction since the flow is still laminar at the reference length and if measured farther downstream an even higher net drag reduction would have been obtained.

The present proof of concept of the possibility to consecutively delay the transition to turbulence with reinforced passive flow control is believed to create an opportunity for future smart surfaces, which in a cheap way can preserve a laminar flow and reduce skin-friction drag. This result can lead to an unforeseen impact on the broad spectrum of industrial applications where reducing drag is a daily challenge. Future work should partly be directed at the stability analysis behind an array of MVGs in order to reveal the underlying behavior of the unstable modes, which are responsible for the breakdown to turbulence. This type of information would be valuable in the optimization and design process of the MVGs with subsequent arrays, necessary for approaching real flow applications.

J.H.M.F. acknowledges the European Research Council for its financial support of the AFRODITE project through a Starting Independent Researcher Grant.

[1] J. H. M. Fransson, A. Talamelli, L. Brandt, and C. Cossu, Phys. Rev. Lett. **96**, 064501 (2006).
[2] C. Cossu and L. Brandt, Eur. J. Mech. B **23**, 815 (2004).
[3] W. Tollmien, Nachr. Ges. Wiss. Göttingen Math. Phys. Kl. 21 (1929) [NACA TM 609 (1931)] .
[4] H. Schlichting, ZAMM—Z. Angew. Math. Mech. **13**, 260 (1933).
[5] G. B. Schubauer and H. K. Skramstad, J. Aerosol Sci. **14**, 69 (1947).
[6] Y. S. Kachanov and O. I. Tararykin, Izv. Sib. Otd. Akad. Nauk SSSR, Ser. Tech. Nauk **18**, 9 (1987).
[7] A. A. Bakchinov, G. R. Grek, B. G. B. Klingmann, and V. V. Kozlov, Phys. Fluids **7**, 820 (1995).
[8] K. J. A. Westin, A. V. Boiko, B. G. B. Klingmann, V. V. Kozlov, and P. H. Alfredsson, J. Fluid Mech. **281**, 193 (1994).
[9] J. H. M. Fransson, L. Brandt, A. Talamelli, and C. Cossu, Phys. Fluids **17**, 054110 (2005).

[10] C. Cossu and L. Brandt, Phys. Fluids **14**, L57 (2002).
[11] P. Schlatter, E. Deusebio, R. de Lange, and L. Brandt, Int. J. Flow Contr. **2**, 259 (2010).
[12] P. Andersson, L. Brandt, A. Bottaro, and D. S. Henningson, J. Fluid Mech. **428**, 29 (2001).
[13] J. H. M. Fransson and A. Talamelli, J. Phys.: Conf. Ser. **318**, 032008 (2011).
[14] J. H. M. Fransson and A. Talamelli, J. Fluid Mech. **698**, 211 (2012).
[15] S. Shahinfar, S. S. Sattarzadeh, J. H. M. Fransson, and A. Talamelli, Phys. Rev. Lett. **109**, 074501 (2012).
[16] S. Shahinfar, J. H. M. Fransson, S. S. Sattarzadeh, and A. Talamelli, J. Fluid Mech. **733**, 1 (2013).
[17] S. Camarri, J. H. M. Fransson, and A. Talamelli, in *Progress in Turbulence V*, edited by A. Talamelli, M. Oberlack, and J. Peinke (Springer, Berlin, 2013), pp. 65–69.
[18] M. V. Morkovin, in *Viscous Drag Reduction*, edited by C. S. Wells (Plenum, New York, 1969).
[19] F. E. Fish, in Proceedings of the International Symposium on Seawater Drag Reduction, Newport, RI, 1998, edited by J. C. S. Meng, pp. 443–450 (unpublished).
[20] Y. C. Jung and B. Bhushan, J. Phys.: Condens. Matter **22**, 035104 (2010).
[21] J. H. M. Fransson, M. Matsubara, and P. H. Alfredsson, J. Fluid Mech. **527**, 1 (2005).